Impaired folate binding of soybean SHMT8 underlies resistance to the soybean cyst nematode

David A. Korasick,[1] Pramod K. Kandoth,[3,4] John J. Tanner,[1,2] Melissa G. Mitchum,[3,5] Lesa J. Beamer[1,2,*]

[1]Department of Biochemistry, University of Missouri, Columbia, Missouri

[2]Department of Chemistry, University of Missouri, Columbia, Missouri

[3]Division of Plant Sciences and Bond Life Sciences Center, University of Missouri, Columbia, Missouri

[4]Current address: National Agri-food Biotechnology Institute, Mohali, Punjab, India

[5]Current address: Department of Plant Pathology and Institute of Plant Breeding, Genetics, and Genomics, Center of Applied Genetic Technologies, University of Georgia, Athens, Georgia

Contents

Supplemental Methods

SEC-MALS-SAXS data acquisition and analysis. SAXS experiments were performed at the Advanced Photon Source Sector 18-ID (Argonne National Lab, Chicago, IL, USA) using a 3.5 m camera. This camera distance allowed acquisition of data in the q range of ~0.005 – 0.38 $Å^{-1}$. His-tagged Essex and Forrest SHMT8 samples were loaded onto a Wyatt SEC WTC 030 S5 column (1.25 MDa exclusion limit) under the control of an Infinity II HPLC unit (Agilent, Santa Clara, CA, USA) with a flow rate of 0.8 mL min^{-1}. The initial load protein concentration was 8 mg mL^{-1} (~150 μM). The MALS instrument was fitted with a Wyatt DAWN Helios II QELS detector and a Wyatt Optilab T-rEX dRI detector (Wyatt, Goleta, CA, USA), was positioned between the HPLC UV monitor and the SAXS flow cell. Sample elution and SAXS data acquisition (0.5 s exposures collected every 3 s) occurred concurrently. MALS data were processed using the ASTRA software package (Wyatt, Goleta, CA, USA) and the SAXS data were reduced to $I(q)$ vs. q curves ($q = 4\pi\sin\theta / \lambda$, where 2θ = scattering angle and $\lambda = 1.03$ Å). Baseline exposures separated from the elution peak were averaged to generate the $I(q)$ vs. q buffer curve. This buffer curve was subtracted from curves within the elution peak to obtain the buffer-subtracted SAXS curve. These experimental SAXS curves were processed and averaged using ATSAS (1).

Guinier analysis was performed using PRIMUS (2). The theoretical scattering curves for the tetrameric crystal structure models of Essex and Forrest SHMT8 and the goodness-of-fit parameter (χ^2) were calculated using FoXS (3). DAMMIF (4) was used for shape reconstruction from the experimental SAXS data. A total of 25 models were independently calculated with enforcement of a P2 symmetry operator. These models were averaged and filtered with DAMAVER (5). The averaged and filtered dummy atom model was superimposed onto the crystallographic tetramer using supcomb (6). The pdb2vol utility of situs (7) was used to convert dummy atom models into volumetric maps.

Analytical ultracentrifugation. Samples for sedimentation equilibrium analysis of Essex and Forrest SHMT8 were run over a Superdex 13/300 SEC column, concentrated, and dialyzed overnight against 50 mM HEPES (pH 7.5), 50 mM NaCl, 0.5 mM TCEP, and 5% (v/v) glycerol. Sedimentation equilibrium experiments were performed in a Beckman XL-I analytical ultracentrifuge using a six-sector charcoal-Epon centerpiece. Reference buffer and protein samples were loaded into a sedimentation equilibrium cell bearing a six-sector charcoal-Epon centerpiece. The experiment utilized three protein concentrations 0.2 mg mL^{-1}, 0.4 mg mL^{-1}, and 0.8 mg mL^{-1} at three rotor speeds – 6,000, 9,000, and 12,000 rpm – collected with the use of an An50Ti rotor at 20°C. Data were collected using absorbance optics monitoring absorbance at 280 nm. Scans included ten replicate measurements. Prior to the first scan, the cell was allowed to equilibrate at 6,000 rpm for 16 h. After this equilibration, scans six total scans were collected at hourly intervals. For data collection at 9,000 and 12,000 rpm, the sample cell was allowed to equilibrate for eight hours followed by acquisition of six scans collected at hourly intervals. The final (sixth) scan from each rotor speed was used for data analysis. Single-body fit calculations were carried out as previously described (8) using Origin 2018.

Table S1. Summary of X-ray data sets collected for Essex SHMT8

	Essex SHMT8•PLP	Essex SHMT8•PLP-Gly	Essex SHMT8• PLP-Gly•FTHF
Space group	$P22_12_1$	$P22_12_1$	$P2_1$
Beamline	ALS 4.2.2	ALS 5.0.2	ALS 4.2.2
Unit cell parameters (Å,°)	a = 55.6, b = 126.8, c = 128.6	a = 56.6, b = 124.6, c = 129.1	a = 86.9, b = 90.8, c = 146.8, β = 90.8
Wavelength (Å)	1.000	1.000	1.000
Resolution (Å)	47.37 - 1.85 (1.89-1.85)	47.84 – 2.10 (2.16 – 2.10)	47.95 – 1.40 (1.42 – 1.40)
Observations[a]	957,925	353,156	1,533,812
Unique reflections	78,106	54,101	440,251
$R_{merge}(I)$[a]	0.097 (1.924)	0.131 (1.658)	0.058 (0.869)
$R_{meas}(I)$[a]	0.106 (2.284)	0.156 (1.967)	0.078 (1.163)
$R_{pim}(I)$[a]	0.041 (1.218)	0.083 (1.043)	0.052 (0.670)
Mean I/σ[a]	19.2 (0.8)	10.5 (1.1)	10.2 (1.0)
Completeness (%)[a]	99.6 (99.7)	99.9 (100.0)	98.5 (98.9)
Multiplicity[a]	12.3 (6.7)	6.5 (6.5)	3.5 (3.2)
No. of protein residues	920	926	1887
No. of protein atoms	6983	7112	14686
No. of LLP atoms	48	N/A	N/A
No. of PLG atoms	N/A	40	80
No. of FFO atoms	N/A	N/A	272
No. of EDO atoms	4	8	68
No. of waters	382	269	1713
R_{cryst}[a]	0.199	0.176	0.164
R_{free}[a,b]	0.231	0.232	0.194
rmsd bonds (Å)	0.007	0.007	0.005
rmsd angles (°)	0.909	0.939	0.858
Ramachandran plot[c]			
Favored (%)	97.68	97.04	97.50
Outliers (%)	0.00	0.00	0.05
Clashscore (PR)[c]	2.67 (99)	2.62 (99)	1.27 (99)
MolProbity score (PR)[c]	1.16 (99)	1.23 (100)	0.94 (100)
Average B (Å^2)	35.0	44.0	19.0
Protein	35.2	44.3	18.2
LLP	35.3	N/A	N/A
PLG	N/A	40.6	12.5
FFO	N/A	N/A	16.3
EDO	36.6	53.2	29.1
Water	40.7	39.5	45.0
Coord. error (Å)[d]	0.27	0.26	0.17
PDB code	6UXH	6UXI	6UXJ

[a]Values for the outer resolution shell of data are given in parenthesis. [b]5% test set. [c]From MolProbity. The percentile ranks (PR) for Clashscore and MolProbity score are given in parentheses. [d]Maximum likelihood-based coordinate error estimate from PHENIX.

Table S2. Summary of X-ray data sets collected for Forrest SHMT8

	Forrest SHMT8•PLP	Forrest SHMT8•PLP-Gly
Space group	$P22_12_1$	$P22_12_1$
Beamline	ALS 4.2.2	ALS 4.2.2
Unit cell parameters (Å,°)	a = 56.1, b = 128.0, c = 128.0	a = 55.7, b = 127.4, c = 127.7
Wavelength (Å)	1.000	1.000
Resolution (Å)	47.70 – 2.10 (2.16 – 2.10)	47.34 – 2.35 (2.43 – 2.35)
Observations[a]	1,094,603	276,672
Unique reflections	54,674	38,087
$R_{merge}(I)$[a]	0.098 (2.733)	0.139 (2.021)
$R_{meas}(I)$[a]	0.103 (2.950)	0.162 (2.399)
$R_{pim}(I)$[a]	0.031 (1.073)	0.083 (1.278)
Mean I/σ[a]	26.4 (0.8)	11.2 (0.8)
Completeness (%)[a]	99.9 (99.8)	100.0 (100.0)
Multiplicity[a]	20.0 (14.2)	7.1 (6.7)
No. of protein residues	924	922
No. of protein atoms	7012	6982
No. of LLP atoms	48	N/A
No. of PLG atoms	N/A	40
No. of EDO atoms	8	N/A
No. of waters	196	85
R_{cryst}[a]	0.181	0.210
R_{free}[a,b]	0.225	0.242
rmsd bonds (Å)	0.008	0.002
rmsd angles (°)	1.001	0.567
Ramachandran plot[c]		
Favored (%)	97.25	97.69
Outliers (%)	0.22	0
Clashscore (PR)[c]	3.46 (99)	4.08 (99)
MolProbity score (PR)[c]	1.48 (98)	1.43 (99)
Average B (Å^2)	54.0	54.0
Protein	54.2	54.6
LLP	63.2	N/A
PLG	N/A	69.5
EDO	60.2	N/A
Water	36.4	45.1
Coord. error (Å)[d]	0.28	0.32
PDB code	6UXK	6UXL

[a]Values for the outer resolution shell of data are given in parenthesis. [b]5% test set. [c]From MolProbity. The percentile ranks (PR) for Clashscore and MolProbity score are given in parentheses. [d]Maximum likelihood-based coordinate error estimate from PHENIX.

Table S3. Structural Parameters from AUC, SAXS, and MALS

	Essex SHMT8	Forrest SHMT8
M_r (Theoretical, tetramer)	213 kDa	216 kDa
M_r – AUC[b]	202 ± 1 kDa (-5%)	202 ± 3 kDa (-6%)
M_r - MALS (Discrepancy)	198 kDa (-7%)	198 kDa (-8%)
M_r – SAXS[c] (Discrepancy)	192 kDa (-10%)	198 kDa (-8%)
R_h - MALS	57 ± 2 Å	58 ± 2 Å
R_g - SAXS	40.3 ± 0.2 Å	41.2 ± 0.2 Å
FoXS R_g	38.8 Å	38.8 Å
FoXS Tetramer Fit χ^2	1.1	1.3

[a]Molecular mass (M_r)
[b]Single body fit M_r from sedimentation equilibrium
[c]M_r from SAXS MoW (9)

Supplemental Figures

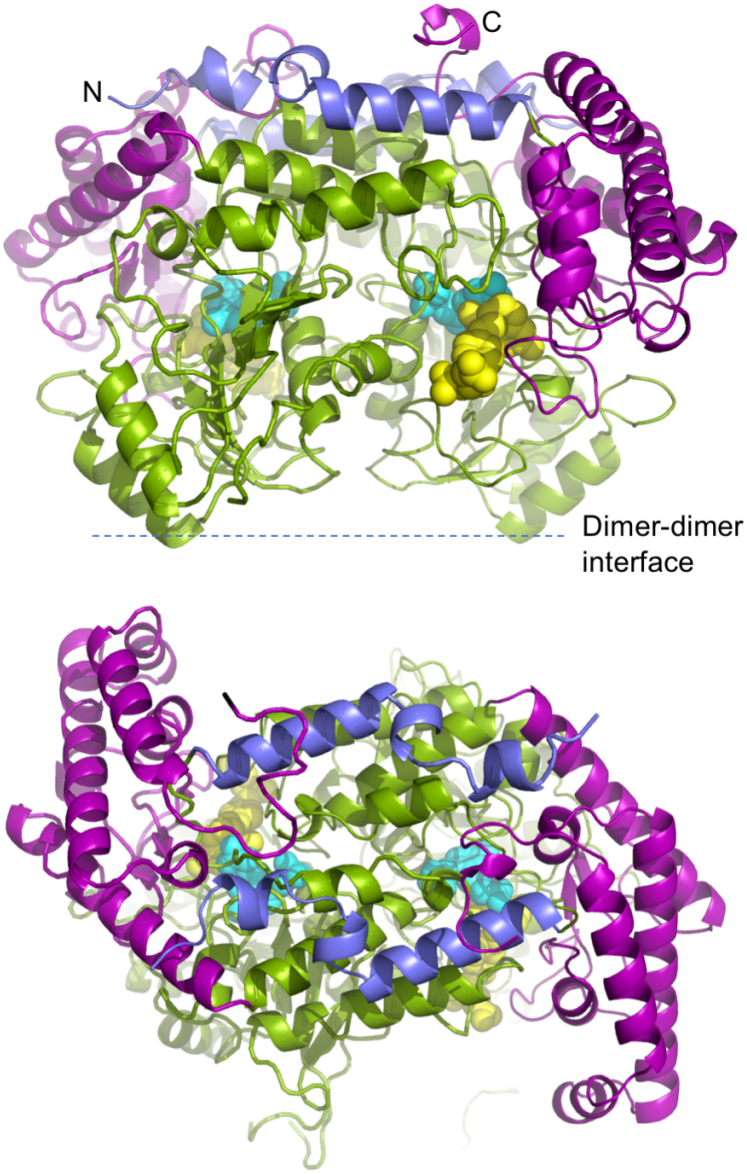

Fig. S1. Two views (related by 90° rotation) of the obligate dimer from Essex SHMT8•PLP-Gly•FTHF. The N-terminal arm (residues 1-32) is blue, the large domain (residues 33-308) is green, and the small domain (residues 309-470) is violet. PLP-Gly (cyan) and FTHF (yellow) are shown as spheres.

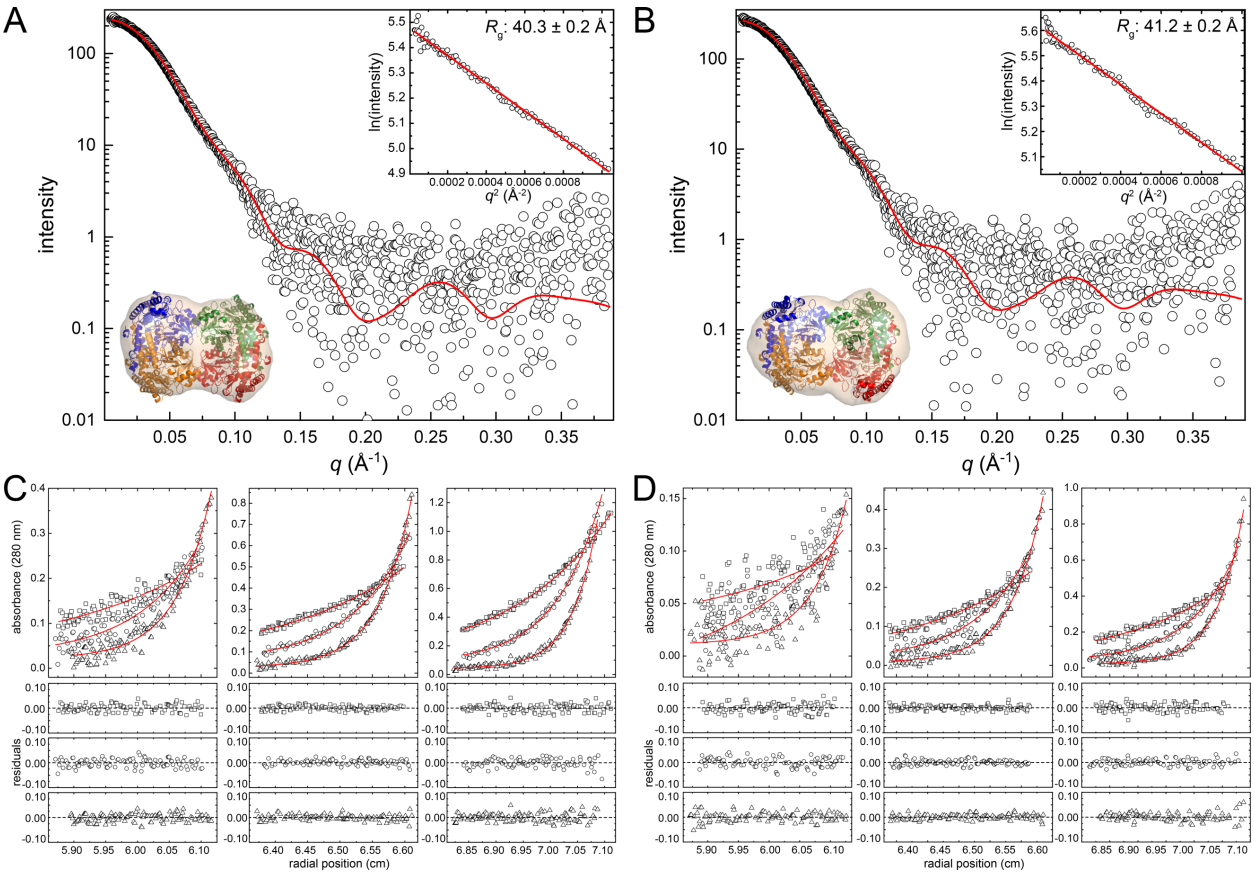

Fig. S2. SAXS and analytical ultracentrifugation studies of SHMT8. SEC-SAXS raw data (open circles) and FoXS fits (red) to a canonical SHMT tetramer assembly for Essex (A) and Forrest (B) SHMT8. The inset in the lower left corner in (A) and (B) shows a shape reconstruction from the experimental SAXS data superimposed with the tetramer crystal structure assembly of Essex or Forrest SHMT8. The upper right hand corner inset shows the Guinier plot of the data. Sedimentation equilibrium data for Essex (C) and Forrest (D) SHMT8 collected at three different protein concentrations: 0.2 mg mL^{-1}, 0.4 mg mL^{-1}, and 0.8 mg mL^{-1}. The symbols in the panels correspond to different centrifugation speeds: 6000 rpm (circles), 9000 rpm (squares), and 12,000 rpm (triangles). The curves represent a global fit of the data to a single-body fit model. Structural parameters derived from these data are included in Table S3.

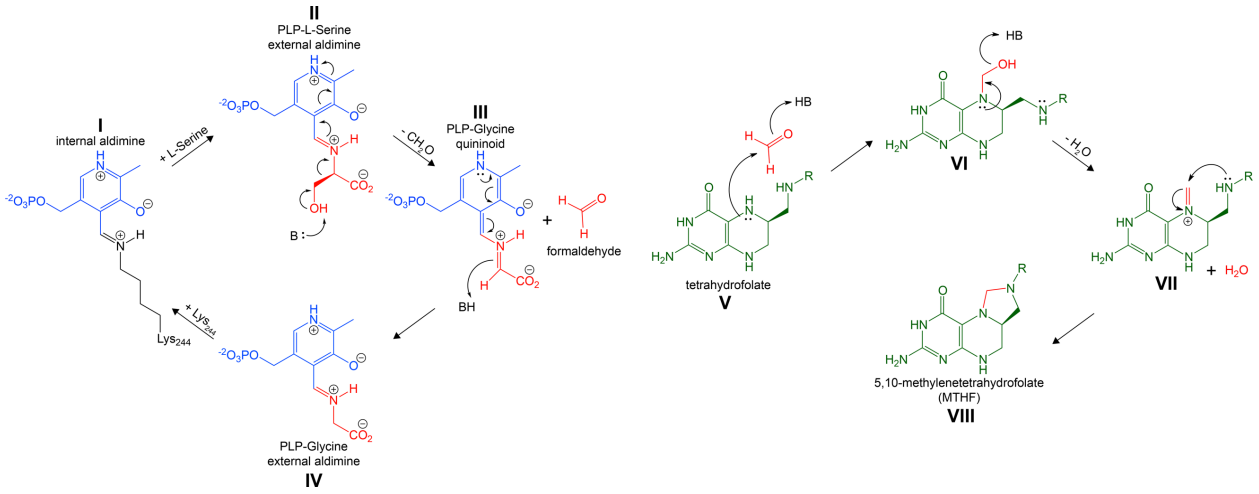

Fig. S3. The basic catalytic mechanism of SHMT. The Schiff base linkage of the PLP internal aldimine with SHMT8 Lys244 (I) is attacked by L-serine to generate the PLP-L-Serine external aldimine (II). A general base in the active site deprotonates the side chain of the PLP-L-Serine, thereby liberating formaldehyde and producing the PLP-glycine quininoid intermediate (III), which through resonance and proton retransfer generates the PLP-glycine external aldimine (IV). The original PLP-Lys244 internal aldimine is regenerated when Lys244 attacks the Schiff base linkage in (IV). The formaldehyde generated in the previous step is attack by the N5 atom of tetrahydrofolate (V). Through a series of proton transfers and internal rearrangements (VI and VII), the product 5,10-methylenetetrahydrofolate (VIII) is produced.

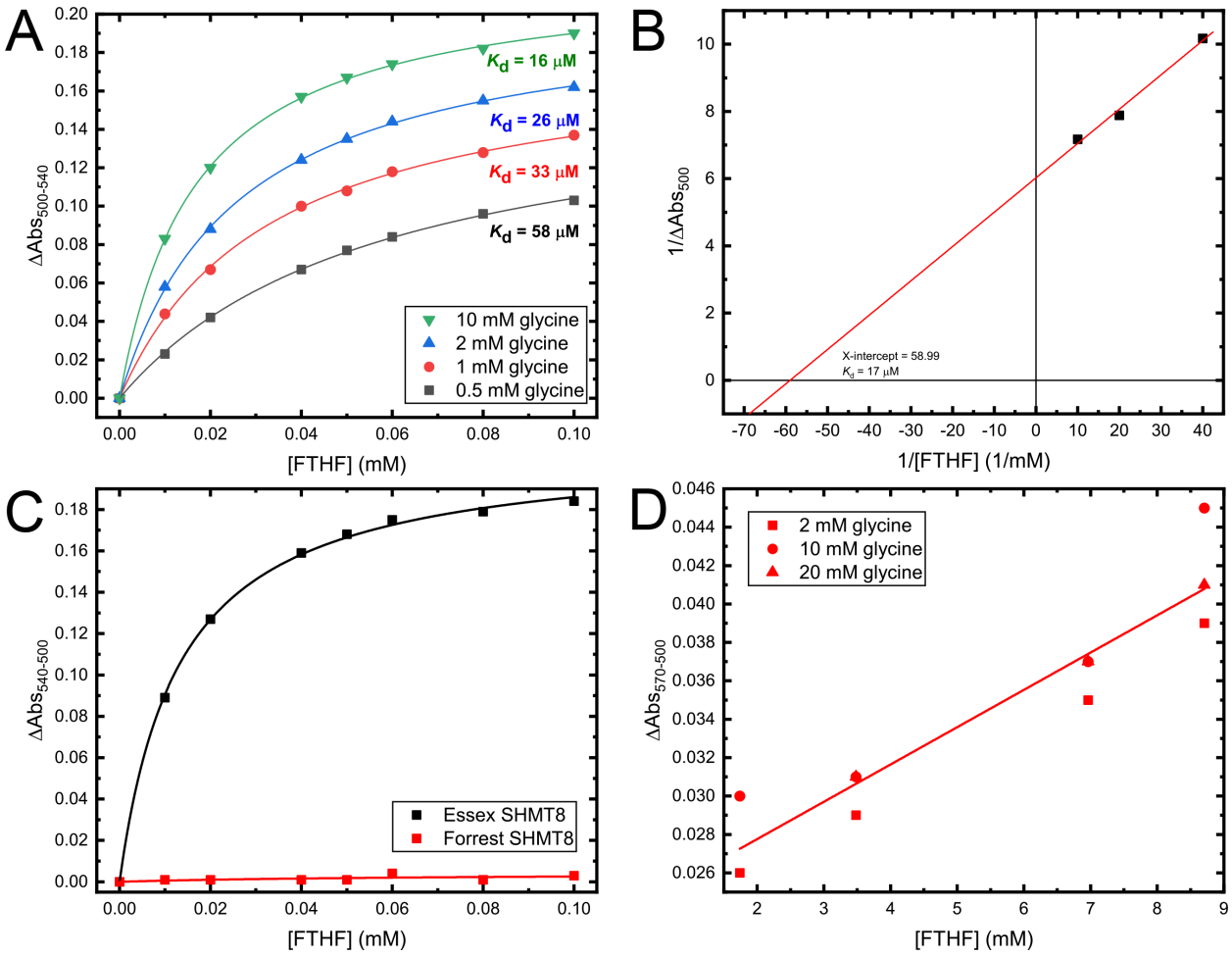

Fig. S4. Data for the Essex and Forrest FTHF Absorbance Binding Assay. (A) Michaelis-Menten fits to the absorbance binding data for Essex SHMT8 as a function of both glycine and FTHF concentrations. The binding affinity for FTHF increases as a function of glycine concentration. (B) Data from the same assay plotted as a double reciprocal plot as described in (10) and (11). We note that the K_d determined from this method matches with the K_d from the highest concentration of glycine in panel (A). (C) A comparison of FTHF binding between Essex and Forrest SHMT8 (black and red, respectively). Both curves are at a saturating concentration of 20 mM glycine. (D) Forrest SHMT8 binds FTHF, however the data do not show hyperbolic behavior, suggesting the enzyme cannot be saturated with FTHF. Additionally, the affinity for FTHF does not appear to be dependent on the concentration of glycine. Please note the difference in magnitude of the y- and x-axes in (D) compared to (C).

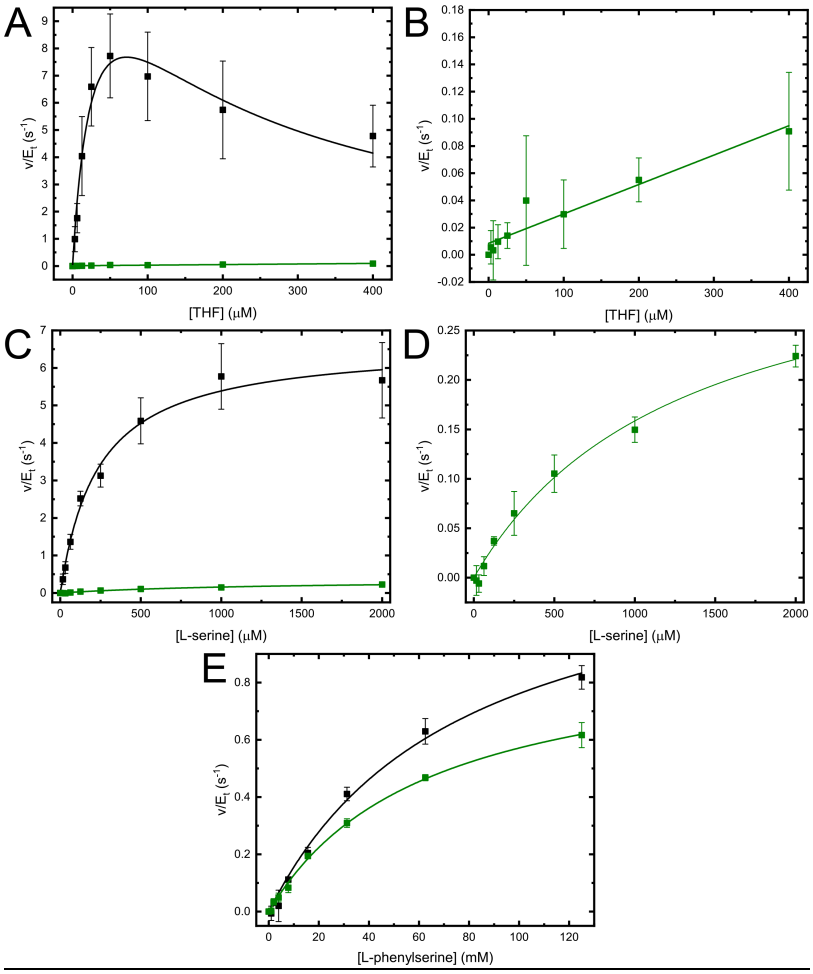

Fig S5. Various kinetics plots and fits to the averaged data for Essex and Forrest SHMT8. (A) Fits from the MTHFD coupled assay where THF is the varied substrate at a fixed concentration of L-serine (2 mM). The Essex SHMT8 dataset was fit to a substrate inhibition model, whereas the Forrest SHMT8 data were fit to a linear regression model. (B) This panel shows a zoomed in version of the Forrest SHMT8 data from panel (A) to more clearly depict the linear dependence. (C) Fits from the MTHFD coupled assay where L-serine is the varied substrate at a fixed concentration of THF (0.4 mM). Both datasets from Essex and Forrest SHMT8 were fit to the Michaelis-Menten equation. (D) This panel shows a zoomed in version of the Forrest SHMT8 data from panel (D) to more clearly depict the Michaelis-Menten behavior of the data.

REFERENCES

1. Franke, D., Petoukhov, M. V., Konarev, P. V., Panjkovich, A., Tuukkanen, A., Mertens, H. D. T., Kikhney, A. G., Hajizadeh, N. R., Franklin, J. M., Jeffries, C. M., and Svergun, D. I. (2017) ATSAS 2.8: a comprehensive data analysis suite for small-angle scattering from macromolecular solutions. *J Appl Crystallogr* **50**, 1212-1225
2. Konarev, P. V., Volkov, V. V., Sokolova, A. V., Koch, M. H. J., and Svergun, D. I. (2003) PRIMUS: a Windows PC-based system for small-angle scattering data analysis. *J. Appl. Crystallogr.* **36**, 1277-1282
3. Schneidman-Duhovny, D., Hammel, M., Tainer, J. A., and Sali, A. (2016) FoXS, FoXSDock and MultiFoXS: Single-state and multi-state structural modeling of proteins and their complexes based on SAXS profiles. *Nucleic Acids Res* **44**, W424-429
4. Franke, D., and Svergun, D. I. (2009) DAMMIF, a program for rapid ab-initio shape determination in small-angle scattering. *J. Appl. Cryst.* **42**, 342-346
5. Volkov, V. V., and Svergun, D. I. (2003) Uniqueness of ab initio shape determination in small-angle scattering. *J. Appl. Crystallogr.* **36**, 860-864
6. Kozin, M. B., and Svergun, D. I. (2001) Automated matching of high- and low-resolution structural models. *J. Appl. Crystallogr.* **34**, 33-41
7. Wriggers, W. (2010) Using Situs for the integration of multi-resolution structures. *Biophys. Rev.* **2**, 21-27
8. Korasick, D. A., Tanner, J. J., and Henzl, M. T. (2017) Impact of disease-Linked mutations targeting the oligomerization interfaces of aldehyde dehydrogenase 7A1. *Chem Biol Interact* **276**, 31-39
9. Piiadov, V., Ares de Araujo, E., Oliveira Neto, M., Craievich, A. F., and Polikarpov, I. (2019) SAXSMoW 2.0: Online calculator of the molecular weight of proteins in dilute solution from experimental SAXS data measured on a relative scale. *Protein Sci* **28**, 454-463
10. Florini, J. R., and Vestling, C. S. (1957) Graphical determination of the dissociation constants for two-substrate enzyme systems. *Biochim Biophys Acta* **25**, 575-578
11. Schirch, L., and Ropp, M. (1967) Serine transhydroxymethylase. Affinity of tetrahydrofolate compounds for the enzyme and enzyme-glycine complex. *Biochemistry* **6**, 253-257